Structural Evaluation of Tibia Bone Under Static Loads Using ANSYS Workbench

¹Chinna Gaunivari Mahesh Babu, ²M Gopalakrishnan, ³K Ganesh, ⁴N Nagesh

¹PG student, Department of Mechanical Engineering, Kuppam Engineering College, India
 ²Assistant Professor, Department of Mechanical Engineering, Kuppam Engineering College, India.
 ³Associate Professor & HOD, Department of Mechanical Engineering, Kuppam Engineering College, India.
 ⁴Associate Professor, Department of Mechanical Engineering, Kuppam Engineering College, India.

Abstract

This study investigates the biomechanical behavior of human tibial cancellous bone under static loading using Finite Element Analysis (FEA) in ANSYS Workbench 2025 R1. A threedimensional tibial model was developed, meshed with high precision, and analyzed under physiologically relevant boundary and loading conditions. Cancellous bone, characterized by its porous and anisotropic structure, was modeled with accurate material properties including young's modulus, density, and Poisson's ratio. The bone was subjected to four load cases: 50 N, 100 N, 150 N, and 200 N. Simulation results showed a linear increase in total deformation, elastic strain, and equivalent (von Mises) stress with increasing load, confirming elastic behavior across the entire range. The maximum deformation and stress values, recorded at 200 N, were 6.3934×10^{-10} m and 1.101 Pa respectively well within the elastic threshold of cancellous bone. Stress and strain concentrations were consistently observed in the middiaphyseal region, identifying it as a critical load-bearing zone. These findings highlight the bone's ability to maintain structural integrity under moderate physiological loads and underscore the effectiveness of FEA in orthopedic analysis. The outcomes of this research offer valuable insights for implant design, fracture risk evaluation, and the optimization of boneimplant interfaces in clinical and biomedical engineering applications.

1.Introduction:

The human tibia is a key load-bearing bone, subjected to significant mechanical forces during activities such as walking, running, and standing. Understanding its biomechanical behavior particularly that of the cancellous (trabecular) bone is vital for improving implant design, fracture management, and prosthetic applications. Cancellous bone, with its porous and anisotropic structure, provides energy absorption and stress distribution despite its lower density and stiffness compared to cortical bone. Accurate modeling of this complex tissue requires advanced tools like Finite Element Analysis (FEA), which has become integral in simulating bone behavior under physiological loading [1-2]. High-resolution anatomical models enhance FEA accuracy, enabling detailed assessments of stress, strain, and deformation patterns [1,3]. This study employs ANSYS 2025 R1 to analyze a tibial model under static loads of 50-200 N, incorporating detailed geometry and material properties. The results revealed a linear increase in deformation, stress, and strain values, indicating elastic behavior within the applied load range consistent with prior findings on sub-yield loading responses [4]. Similar ANSYS-based studies have validated FEA predictions against experimental data, emphasizing its effectiveness in orthopedic biomechanics [5-6]. Realistic boundary conditions, such as fixed distal ends and compressive loads at the tibial plateau, were applied to replicate physiological loading [11]. Material selection significantly affects simulation outcomes. Common implant materials such as stainless steel, titanium alloys, PEEK, and cobalt-chromium are modeled for their distinct mechanical and biocompatible properties [13-19]. These choices influence stress distribution and help optimize implant placement. The heterogeneous nature of bone requires accurate representation of anisotropic properties; homogeneous models may underestimate stress concentrations [10] [20-21]. Additionally, high-resolution CT scans are often used to build precise 3D bone geometries for analysis. While ANSYS provides a powerful platform for biomechanical modeling, challenges remain in capturing bone anisotropy, integrating muscular forces, and ensuring validation with experimental data. Future advancements may include patient-specific models, real-time simulations, and integration with gait dynamics to further enhance orthopedic research and clinical applications.

2. Material Properties: Cancellous Bone Load: 50N

2.1 Geometry:

Figure 2.1 depicts the geometric modeling of a human tibia bone using ANSYS 2023 R1 Student Edition. The image presents a three-dimensional representation of the tibia overlaid with a wireframe mesh, indicating surface discretization in preparation for finite element analysis (FEA).

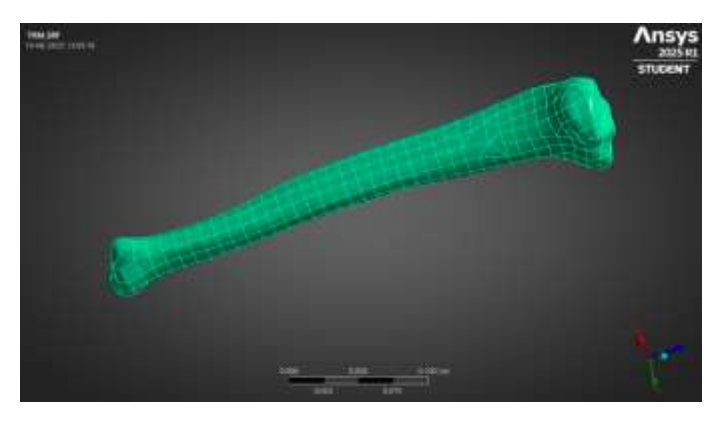


Fig. 2.1. Geometric Modelling of Tibia Bone

This modeling step is fundamental in biomechanical research, as it enables the assessment of stress and strain under various loading scenarios. The anatomically accurate geometry, combined with appropriate meshing, enhances simulation reliability for orthopedic, prosthetic, and trauma-related applications. The use of ANSYS underscores the integration of advanced engineering tools in biomedical analysis.

2.2. Meshing

The fine mesh detail indicates a high-resolution model, which is essential for achieving accurate results in stress, strain, and deformation simulations. Proper meshing ensures that the computational model can capture the complex anatomical features and variations in the tibia's structure. This step is particularly important in biomedical applications where precise prediction of biomechanical behavior under physiological loads is required. The image demonstrates that the meshing was done carefully, with smooth transitions and consistent element sizing to maintain both computational efficiency and solution accuracy.

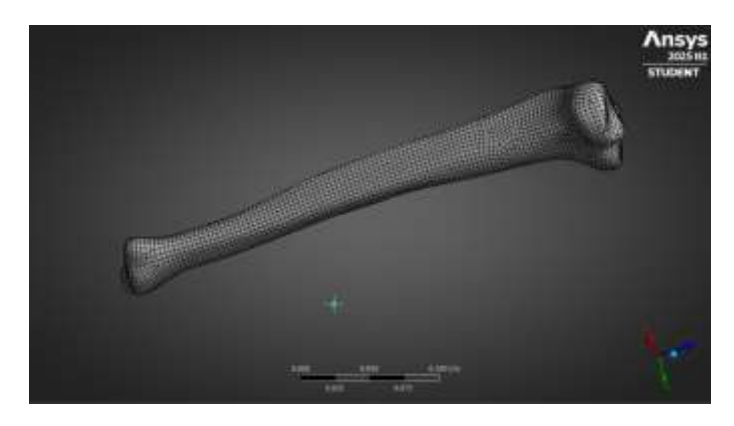


Fig. 2.2. Meshing of Tibia bone

2.3. Boundary Conditions:

Figure 2.3 illustrates the application of boundary conditions to the tibia bone model in ANSYS. In this static structural analysis, a fixed support is applied at the lower end of the tibia, indicated by the blue-highlighted region. This constraint fully restricts both translational and rotational movement, simulating an immobile interface such as the tibia's connection to the ankle. Accurate boundary condition definition is critical in finite element analysis to replicate physiological constraints and loading scenarios. In this context, the fixed support enables realistic simulation of mechanical forces acting on the bone, ensuring reliable predictions of stress distribution and structural behaviour. Such setups are essential for biomechanical assessments, orthopedic implant design, and injury analysis.

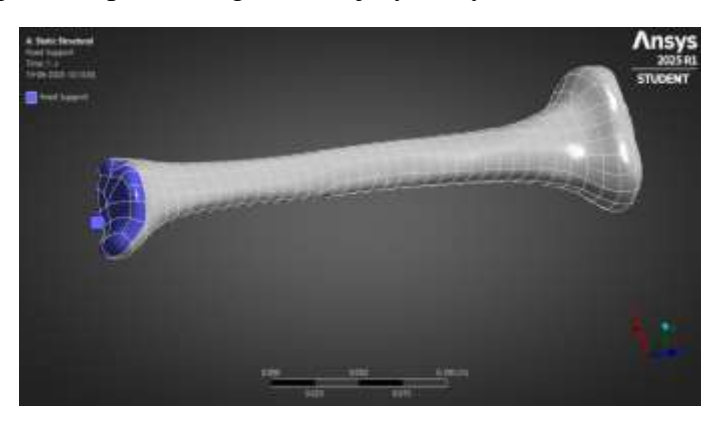


Figure 2.3: Boundary Conditions of the Tibia bone

2.4. Loading Conditions:

Figure 2.4 displays the application of a load on the tibia bone model within a static structural simulation using ANSYS. The red-highlighted region at the upper end of the bone indicates the surface where a pressure load of 50 Pascals is applied. This load simulates external forces such as body weight or muscular action exerted during activities like standing or walking. The applied pressure mimics physiological compressive forces, enabling a realistic assessment of the bone's mechanical behavior. Proper load definition is essential in finite element analysis to evaluate stress distribution, deformation, and failure risk. The figure confirms that the load is correctly oriented and uniformly applied, supporting accurate and meaningful results in biomechanical simulations.

Journal of Engineering and Technology Management 77 (2025)



Figure 2.4: Loads acting on the tibia bone

The material properties used in the finite element analysis of the tibia bone. The table includes three materials: cancellous bone, titanium alloy, and stainless steel 316L, each defined by their Young's Modulus, density, and Poisson's ratio. Cancellous bone, representing the natural spongy structure of the tibia, has a low Young's Modulus of 0.5 GPa, indicating high flexibility. Its density is 300 kg/m³, and a Poisson's ratio of 0.2 reflects moderate lateral deformation under compressive loads.

3. Results and Discussion

3.1 Cancellous bone Material

3.1.1. Total deformation:

Figure 3.1 illustrates the total deformation of cancellous bone under a static structural load of 50 N, simulated using ANSYS 2025 R1 Student Version. The color contour map indicates deformation magnitudes ranging from 0 m (dark blue) to approximately 1.5984×10^{-10} m (bright red). Deformation is non-uniform, with the highest values occurring at the left end likely the load application site while the right end, assumed to be fixed, shows minimal displacement. These results reflect the typical mechanical response of cancellous bone, characterized by small yet measurable deformations due to its porous, compliant structure. The simulation confirms the bone's capacity to bear physiological loads with minimal displacement, aligning with its biomechanical function.

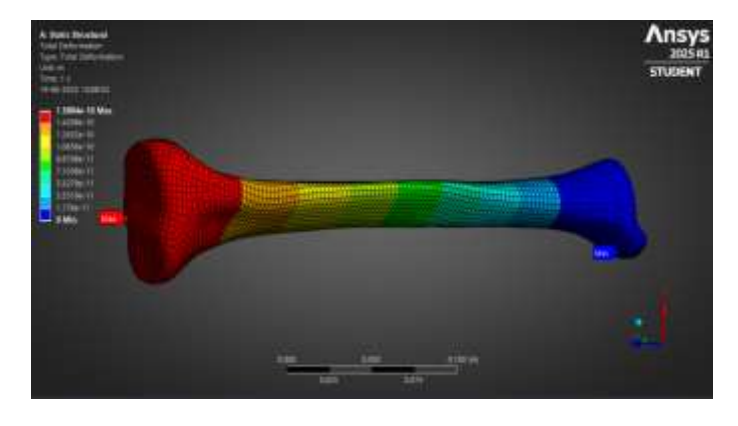


Fig. 3.1 Total Deformation of Cancellous bone Material

3.1.2. Elastic Strain:

Figure 3.2 shows the distribution of equivalent elastic strain in cancellous bone under a static structural load of 50 N, analyzed using ANSYS. Strain values range from 0 m/m (blue) to approximately 5.5317×10^{-10} m/m (red), indicating the extent of elastic deformation within the material. The highest strain concentration appears in the upper right region of the bone (red), suggesting localized stress due to the applied load. In contrast, the lower left region (blue) exhibits minimal strain, likely corresponding to a constrained or less stressed area. The gradual color transition across the model reflects how strain propagates through the structure. These findings align with the anisotropic and heterogeneous characteristics of cancellous bone, where strain distribution varies with internal architecture. The overall low strain values confirm the bone's capacity to deform elastically under physiological loading conditions.

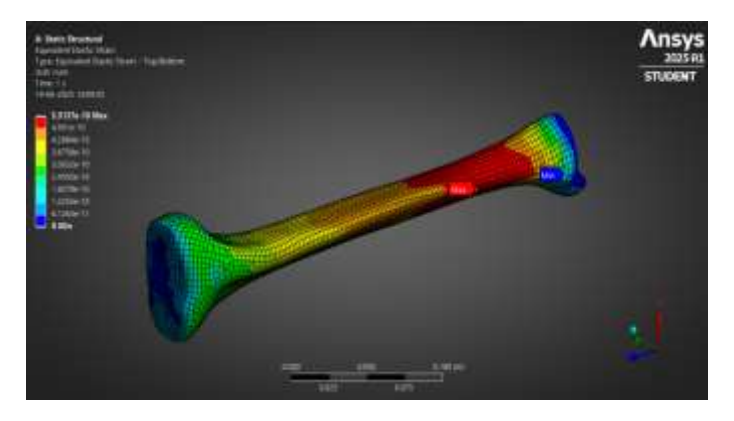


Fig. 3.2 Elastic Strain of Cancellous bone Material

3.1.3. Equivalent Stress:

Figure 4.3 presents the equivalent (von Mises) stress distribution in cancellous bone under a static load of 50 N, analyzed using ANSYS 2025 R1 Student Version. The stress values, expressed in Pascals (Pa), range from 0 Pa (dark blue) to a maximum of approximately 0.27255 Pa (red). This contour plot highlights regions of peak mechanical stress, with the highest concentration observed in the top-right portion of the bone model marked by red coloring and the "Max" label indicating a zone of potential structural vulnerability. In contrast, the lower-left region, shown in blue, experiences minimal stress, likely due to boundary constraints. The smooth color gradient from blue to red illustrates how stress propagates through the bone under load.

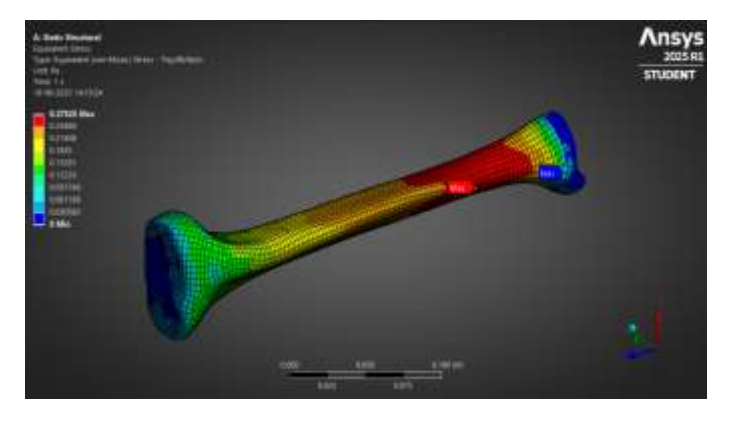


Fig. 4.3 Equivalent Stress of Cancellous bone Material

Although the overall stress magnitudes are low, the distribution pattern reveals critical load-bearing areas and stress concentrations, consistent with the anisotropic, porous nature of cancellous bone. These insights are essential for evaluating biomechanical performance and have implications for implant design, fracture risk assessment, and orthopedic treatment planning.

3.2. Material properties: Cancellous bone

Load: 100N

3.2.1. Total deformation:

Figure 4.6 depicts the total deformation of cancellous bone under a 100 N static load, simulated using ANSYS 2025 R1. Deformation, measured in meters, is visualized through a color gradient from blue (minimum) to red (maximum). The maximum deformation of 3.1976×10^{-10} m occurs at the proximal end (red zone labeled "Max"), where the load is applied, while the minimum deformation appears at the constrained distal end (deep blue, labeled "Min").

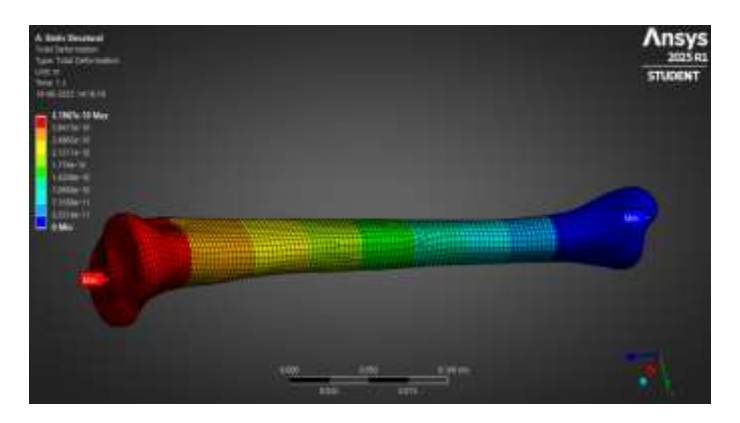


Fig. 4.4 Total Deformation of Cancellous bone Material

The gradual transition of colors along the bone length indicates smooth elastic deformation in response to the axial or bending load. This behavior highlights the bone's capacity to distribute force efficiently, with localized deformation near the loaded region. Such results are crucial for understanding cancellous bone mechanics under physiological loads and have direct applications in orthopedic implant design, fracture risk assessment, and surgical planning.

3.2.2. Strain:

Figure 4.7 shows the equivalent elastic strain distribution in cancellous bone under a $100 \,\mathrm{N}$ load, analyzed using ANSYS $2025 \,\mathrm{R}1$. Strain values, expressed in meters per meter (m/m), range from 0 (blue) to a maximum of $1.1027 \times 10^{-9} \,\mathrm{m/m}$ (red). The region of maximum strain, marked "Max," is located near the mid-shaft of the bone, likely corresponding to a stress concentration due to bending or load application. The minimum strain, marked "Min" in dark blue, appears near the distal end, which is presumably fixed during the simulation. The smooth color gradient from blue to red indicates a gradual and uniform elastic response, demonstrating effective load distribution. The results confirm that the bone remains within its elastic range under a $100 \,\mathrm{N}$ load, undergoing fully reversible deformation. This analysis is vital for

understanding cancellous bone mechanics and supports applications in prosthetic design, fracture risk evaluation, and orthopedic planning.

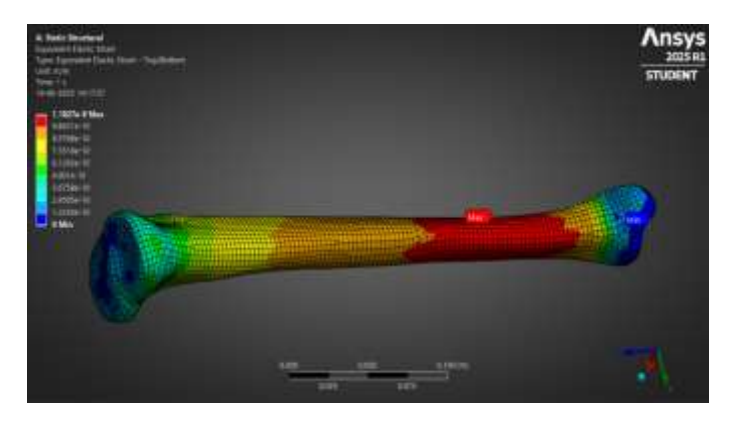


Fig. 4.5 Elastic Strain of Cancellous bone Material

3.2.3. Equivalent Stress:

Figure 4.8 illustrates the equivalent (von Mises) stress distribution in cancellous bone of the tibia under a 100 N load, analyzed using ANSYS 2025 R1. Stress values, shown in Pascals (Pa), range from 0 Pa (blue) to a maximum of 0.55049 Pa (red). The maximum stress, marked "Max," occurs in the mid-diaphyseal region, indicating a critical zone for load transfer and potential stress concentration.

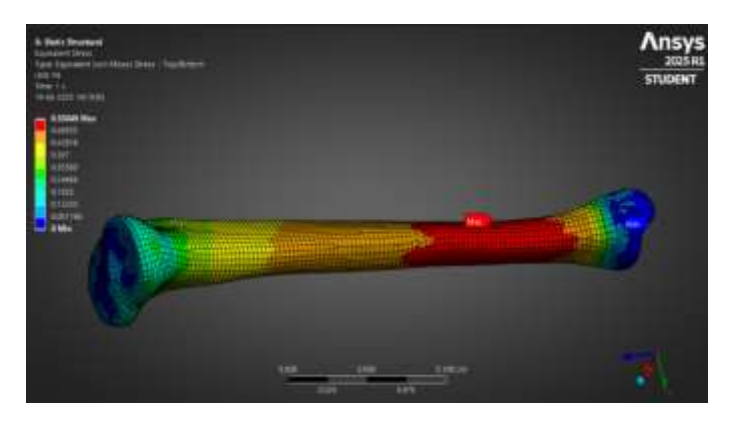


Fig. 4.6 Equivalent Stress of Cancellous bone Material

The minimum stress, labeled "Min" in blue, appears near the constrained distal end, which experiences minimal loading. The smooth gradient from red to blue reflects the bone's capacity to redistribute mechanical loads effectively. This von Mises stress distribution is vital for assessing the bone's resistance to yielding, ensuring structural integrity, and guiding implant design or failure risk evaluations in orthopedic applications.

3.3. Material properties:

Load: 150N

3.3.1. Total deformation:

Figure 4.11 presents the total deformation of cancellous bone under a 150 N load, simulated using ANSYS 2025 R1 in a static structural environment. Deformation is measured in meters (m) and visualized using a color contour ranging from 0 m (blue) to a maximum of 4.7951×10^{-10} m (red). The maximum deformation, labeled "Max," occurs at the proximal end

where the load is applied, while the minimum deformation, labeled "Min," is observed at the fixed distal end.

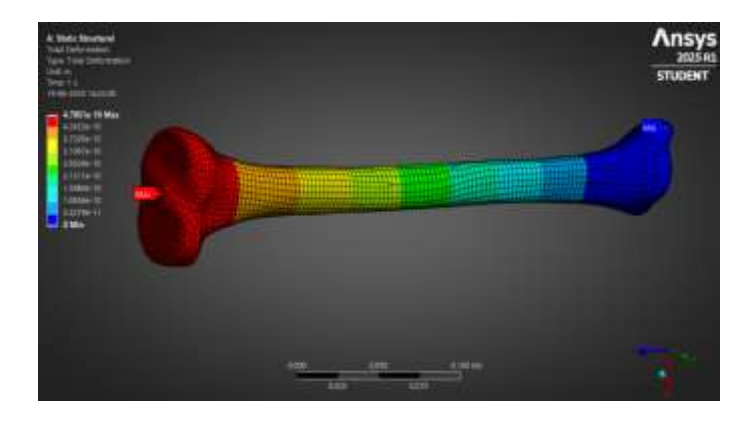


Fig. 4.7 Total Deformation of Cancellous bone Material

The smooth transition from red to blue illustrates the progressive increase in deformation from the constrained to the loaded region. Compared to lower loads, the deformation magnitude increases with the 150 N force, yet remains within the elastic range, indicating no structural failure. This analysis is essential for evaluating the mechanical performance of cancellous bone under higher physiological loads, informing implant design and orthopedic treatment strategies.

3.3.2. Strain:

Figure 4.12 shows the equivalent elastic strain distribution in tibial cancellous bone under a 150 N applied load, simulated using ANSYS 2025 R1. Strain values, measured in m/m, range from 0 m/m (blue) to a maximum of 1.6541×10^{-9} m/m (red). The maximum strain, labeled "Max," is concentrated in the mid-diaphyseal region, indicating the primary zone of deformation under loading.

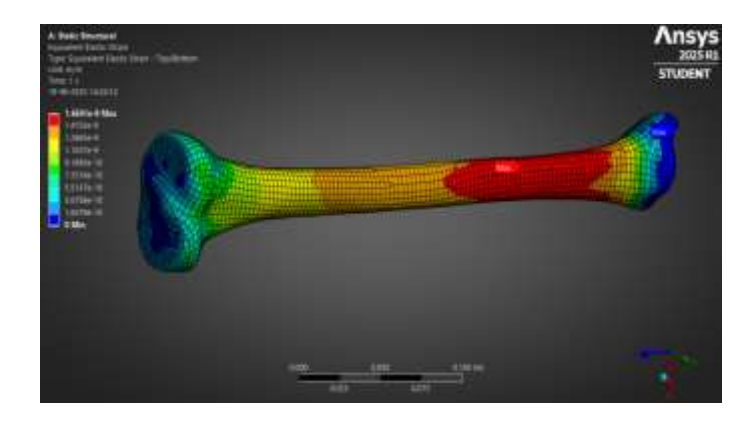


Fig. 4.8 Elastic Strain of Cancellous bone Material

The minimum strain, marked "Min," occurs at the distal end, which serves as the fixed boundary in the simulation and thus undergoes minimal deformation. The smooth gradient from blue to red suggests a uniform strain distribution, increasing toward the loaded end. Compared to lower-load cases, the higher strain values at 150 N confirm continued elastic behavior, with the material remaining within physiological limits. This analysis aids in

assessing strain tolerance for orthopedic implants and understanding cancellous bone response under elevated mechanical loads.

3.3.3. Equivalent Stress:

Figure 4.13 presents the equivalent (von Mises) stress distribution in a cancellous bone model under a static load of 150 N, simulated using ANSYS 2025 R1. Stress values range from a minimum of 0.091749 Pa (blue) to a maximum of 0.82574 Pa (red). The peak stress, labeled "Max," is located on the anterior midshaft, indicating a region of significant load transfer, likely due to bending or compression.

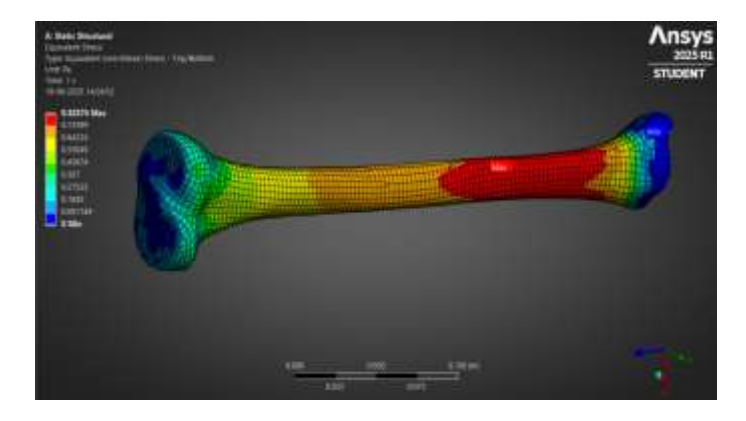


Fig. 4.9 Equivalent Stress of Cancellous bone Material

The lowest stress, labeled "Min," occurs near the distal epiphysis, where mechanical influence is minimal due to boundary constraints. The smooth gradient from high to low stress illustrates how bone geometry and load path influence stress distribution. This analysis is crucial for assessing structural integrity, identifying high-risk zones for fracture, and guiding the design of orthopedic implants under physiological loading conditions.

3.4. Material: Cancellous Bone

Load: 200N

3.4.1. Total deformation:

Figure 4.16 depicts the total deformation of cancellous bone under a 200 N static load, simulated using ANSYS 2025 R1. The deformation, measured in meters, ranges from a minimum of 7.1308×10^{-11} m (deep blue, labeled "Min") at the distal end likely constrained by boundary conditions to a maximum of 6.3934×10^{-10} m (red, labeled "Max") at the proximal end, where the load is applied or where flexibility is highest.

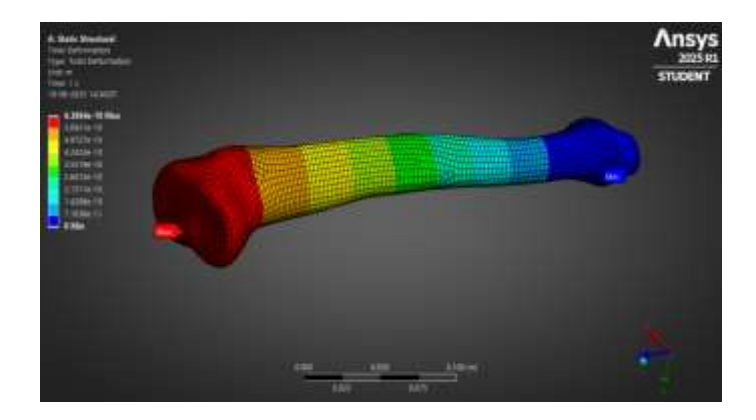


Fig. 4.10 Total Deformation of Cancellous bone Material

The smooth gradient from red to blue reflects a gradual displacement transition along the bone length, consistent with elastic deformation under load. This outcome demonstrates the bone's mechanical compliance and helps identify regions prone to higher deformation. Such findings are essential in orthopedic biomechanics for assessing load-bearing performance, optimizing implant placement, and evaluating fracture risk.

3.4.2. Strain:

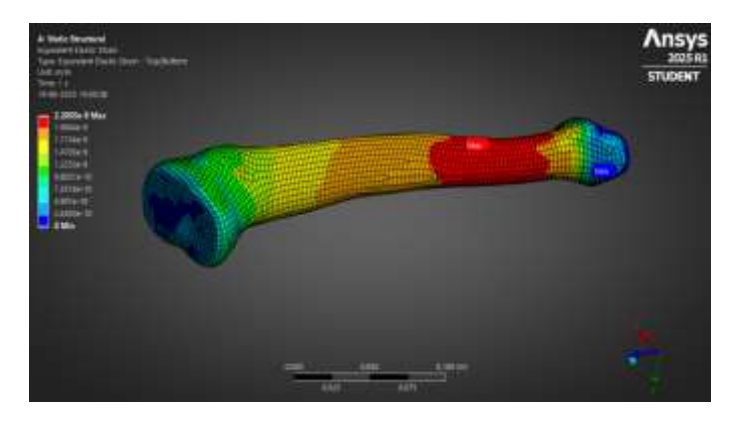


Fig. 4.11 elastic strain of Cancellous bone Material

3.4.3. Equivalent Stress:

Figure 4.17 presents the equivalent elastic strain distribution in cancellous bone under a static load of 200 N, as simulated in ANSYS 2025 R1. The strain, expressed in meters per meter (m/m), reflects the degree of elastic deformation across the bone. A maximum strain of approximately 2.2055×10^{-9} m/m is observed in the mid-diaphyseal region (highlighted in red and marked "Max"), indicating areas of heightened mechanical response due to bending or compressive forces. Conversely, the minimum strain, around 2.4550×10^{-10} m/m, appears near the distal end (deep blue, labeled "Min"), where deformation is minimal due to boundary constraints.

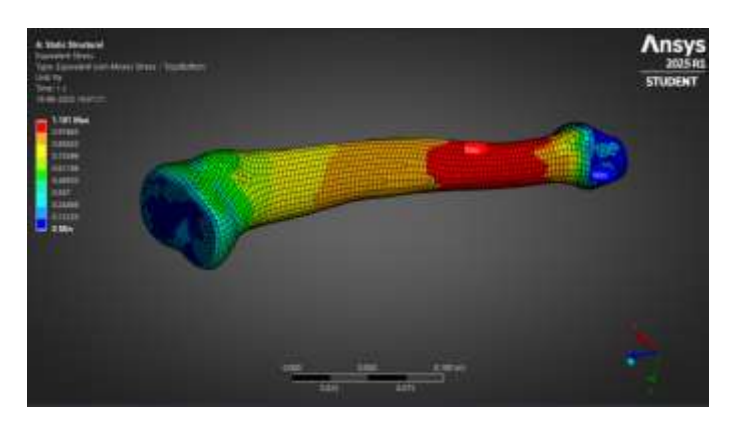


Fig. 4.12 Equivalent stress of Cancellous bone Material

The gradual color transition from blue through green and yellow to red illustrates a smooth strain distribution along the shaft, highlighting zones of increasing elastic response. This pattern underscores the bone's structural adaptability under higher loads and provides valuable

insight into stress-bearing behavior, implant design optimization, and the biomechanics of load transfer in cancellous bone.

Table 4.5 Stress, strain, and total deformation of Cancellous bone material

Load, N	50	100	150	200
Total Deformation, m	1.5984 × 10 ⁻¹⁰	3.1976×10^{-10}	4.7951×10^{-10}	6.3934×10^{-10}
Elastic Strain	5.5317 × 10 ⁻¹⁰	1.1027×10^{-9}	1.6541×10^{-9}	2.2055×10^{-9}
Equivalent Stress. Pa	0.27255	0.55049	0.82574	1.101

Table 4.5 presents the results of a static structural analysis performed on cancellous bone material under varying axial loads of 50 N, 100 N, 150 N, and 200 N, using ANSYS 2025 R1. The table summarizes three key mechanical parameters: total deformation (in meters), elastic strain (in m/m), and equivalent (von Mises) stress (in Pascals). As the applied load increases, a consistent and nearly linear rise is observed across all parameters. Total deformation increases from 1.5984×10^{-10} m at 50 N to 6.3934×10^{-10} m at 200 N, indicating a proportional displacement response of the bone under load. Similarly, the elastic strain rises from 5.5317×10^{-10} m/m to 2.2055×10^{-9} m/m across the same load range, demonstrating increased internal deformation. The equivalent stress also shows a corresponding growth, doubling approximately with each load increment from 0.27255 Pa at 50 N to 1.101 Pa at 200 N indicating the development of stress within safe elastic limits. This table highlights the bone's predictable and elastic mechanical behavior under increasing physiological loads, which is essential for orthopedic implant design, load-bearing assessment, and biomechanical modeling.

4. Conclusion:

The finite element analysis of cancellous bone under varying static loads using ANSYS Workbench has yielded valuable insights into its biomechanical response and structural performance. By applying axial loads ranging from 50 N to 200 N, the study systematically evaluated key parameters such as total deformation, elastic strain, and equivalent (von Mises) stress. The results confirmed that cancellous bone behaves in a linear elastic manner throughout the tested range, with proportional increases in all mechanical responses corresponding to increased loading. The stress and strain were consistently concentrated in the mid-diaphyseal region, validating its role as a primary load-bearing zone in the tibia. Despite the increasing loads, the deformation and stress values remained within the microscale and well below failure thresholds, indicating excellent elastic resilience of the cancellous bone structure. These outcomes not only affirm the load-distribution efficiency of trabecular architecture but also support the safe application of such simulations for orthopedic implant evaluation, fracture risk analysis, and prosthetic development. Overall, the study highlights the utility of FEA as a non-

invasive, cost-effective tool for simulating physiological loading conditions and guiding the optimization of biomedical designs. Future research incorporating patient-specific geometries, dynamic loading conditions, and bone-implant interaction modeling could further enhance the clinical relevance of these simulations.

5. References

- [1]. Viceconti, M., Olsen, S., Nolte, L. P., & Burton, K. (2005). Extracting clinically relevant data from finite element simulations. Clinical Biomechanics, 20(5), 451–454.
- [2]. Pistoia, W., van Rietbergen, B., Lochmüller, E. M., Lill, C. A., Eckstein, F., & Rüegsegger, P. (2002). Estimation of distal radius failure load with micro-finite element analysis models based on three-dimensional peripheral quantitative computed tomography images. Bone, 30(6), 842–848.
- [3]. Akkus, O., & Rimnac, C. M. (2020). Biomechanics of bone. Comprehensive Biomaterials II. Elsevier.
- [4]. Cowin, S.C. (2001). Bone Mechanics Handbook. CRC Press.
- [5]. Silva, M.J., et al. (1998). Finite element analysis of the femoral neck: Accuracy of bone geometry and material property representation. Journal of Biomechanics, 31(4), 317-329.
- [6]. Nazarian, A., & Müller, R. (2004). Time-lapsed microstructural imaging of bone failure behavior. Journal of Biomechanics, 37(1), 55-65.
- [7]. Wirtz, D.C., et al. (2000). Experimental and computational evaluation of a new implant design for vertebral body replacement, Journal of Biomechanics, 33(11), 1399-1407.
- [8]. Viceconti, M., et al. (2005). Biomechanics modeling of the musculoskeletal system in orthopaedic surgery planning, Clinical Biomechanics, 20(9), 1013-1018.
- [9]. Maheshwari, R. S., et al. (2020). Finite Element Analysis of Tibia Bone under Static Loading Condition Using ANSYS Workbench, International Journal of Engineering Research & Technology (IJERT), 9(5), 789–793.
- [10]. Kotha, S. P., et al. (2001), Anisotropic elastic properties of human cortical bone: Relationship to density and microstructure, Journal of Biomechanics, 34(6), 779–785.
- [11]. Lemaire, T., et al. (2009), Tibia stress evaluation in dynamic gait simulation using FEA, Journal of Biomechanical Engineering, 131(10), 101010.
- [12]. Shah, J., et al. (2018), Biomechanical analysis of osteoporotic tibia using FEA, Computers in Biology and Medicine, 100, 89–97.
- [13]. Naveen Kumar, Irfan G. et al. (2021), A review on tribological behaviour and mechanical properties of Al/Z_rO_2 metal matrix nano composites, Materials Today: Proceedings, Volume 38, Part 5, Pages 2649-2657, ISSN 2214-7853.

- [14]. Naveen Kumar, G. Irfan. et al. (2021), Mechanical, microstructural properties and wear characteristics of hybrid aluminium matrix nano composites (HAMNCs) review, Materials Today: Proceedings, Volume 45, Part 2, Pages 619-625, ISSN 2214-7853.
- [15]. Naveen Kumar., Irfan G., Udayabhanu., G. Nagaraju. et al. (2021), Green synthesis of zinc oxide nanoparticles: Mechanical and microstructural characterization of aluminum nano composites, Materials Today: Proceedings, Volume 38, Part 5, Pages 3116-3124, ISSN 2214-7853.
- [16]. Devaraj, E., Naveen Kumar. et al. (2024), Matrix and Reinforcement for Biopolymer Composites-A Review", Journal of Engineering and Technology Management, Volume 72, 1135-1167.
- [17]. Naveen Kumar, Irfan G. et al. (2021), Tribological behaviour and micro hardness of Al-Si7.0-0.5mg matrix nano composites though stir casting technique, International Journal of Mechanical Engineering and Technology (IJMET), Volume 12, Issue 9, September 2021, pp. 13-20, IAEME publication.
- [18]. Naveen Kumar et al. (2018), Numerical investigation on turbulence effects of delta wing vortex generators on thermal performance of oval fin heat exchanger, Journal of Emerging Technologies and Innovative Research (JETIR), December 2018, Volume 5, Issue 12, pages 150-154.
- [19]. Abhishek H A and Naveen Kumar, et al. (2017), Production of biodiesel and property evaluation from waste coconut oil and performance, emission and combustion characterization using diesel engine, International Journal of Mechanical Engineering and Technology (IJMET), Volume 8, Issue 4, April 2017, pp. 184-193.
- [20]. Naveen Kumar (2025), Investigation on the Cooling Rate and Microstructural Characteristics of Cast Low Melting Alloys, Journal of Engineering and Technology Management 77, 278-289.
- [21]. Lohitesh Jaga Kumar (2025), Effect of Reinforcement Morphology and Composition on the Properties of Aluminum Matrix Composites, Journal of Engineering and Technology Management 77, 337-350.